Sādhanā (2022)47:109
https://doi.org/10.1007/s12046-022-01877-4

Characteristics assessment of local scour encircling twin bridge piers positioned side by side (SbS)

GEETA DEVI* and MUNENDRA KUMAR

Delhi Technological University, New Delhi 110042, India
e-mail: geeta_phd2k17@dtu.ac.in; munendrakumar@dtu.ac.in

MS received 28 August 2021; revised 24 January 2022; accepted 28 March 2022

Abstract. In the case of multiple pier arrangements, commonly used manuals still suggest using methods for an isolated pier, irrespective of the spacing between the pier and the factors influencing the pairs of the pier. The present study is an experimental investigation for assessing maximum scour depth (MSD) characteristics around the twin piers installed in side-by-side (SbS) positioning. Twenty-seven experimental conditions were evaluated for three sets of the rate of flow. The Acoustic Doppler Velocimeter (ADV) was used to precisely measure flow intensity under the clear water condition. Center-to-center (C2C) spacing between the piers was varied from 1.5, 2, 2.5, 3, 3.5, 4, 4.5 to 5 times pier diameter (D). In the vortex region higher amount of turbulence is perceived owing to a stronger horseshoe vortex forming between the piers. This turbulence resulted from various factors influencing the MSD, and these parameters are assessed and formulated by dimensional analysis. The findings of the study demonstrate the effect of Froud number, the effect of dimensional parameters, the effect of sediment deposition, and the effect of C2C spacing between the piers on the pattern of MSD for the two piers. During the comparison of the experimental data with the semi-empirical equations, the best value root mean square and maximum absolute percentage error was observed as 0.97 and 1.5%, respectively, for the Larsen and Toch equation. Bridge pier constitutes numbers of piers, this study will impart new light on mutual interference between the two piers and its effect on the local scouring evolved in the propinquity of the pier, so that the current engineering equations can be modified for the accurate prediction of scouring.

Keywords. Bridge piers; Local scour; Piers-flow interaction; Maximum scour depth; River hydraulics; Side-by-side positioning; Sediment transport.

1. Introduction

As traffic volumes increased in many nations due to fast economic growth, more and more bridges over the rivers and canals have been constructed. The presence of bridge piers affects the local flow field, often leading to the creation of small scouring holes that might harm the corresponding bridge components [1]. Sediment transport is a common phenomenon during flooding. When significant lift force on suspended particles is available to overcome the frictional grips between the particles, sediment suspension will be generated due to the turbulence in the flow [2]. Scour is one of the main problems for efficient management of water resources. Local scour has the potential to cause hydraulic structures like bridge piers, spur dikes, and abutments to collapse [3]. The major source of chorography changes resulting in land loss, exceeding sediment output, and consequent water quality degradation is the scouring processes in water bodies [4]. Owing to the flexibility of the fluid flow structure, the local scouring across the bridge structure is very hard to trace. A precise prediction of bridge MSD prevents bridge failure and effectively reduces overestimated building costs unnecessarily [5]. This is partly responsible for the flow through the piers and their interplay with the sediments in the bed. For over a half-century, several types of research studies have been made to discover scouring around the single pier [6–19]. However, no conflict with any other structure present in the encircling area was considered in such experiments.

In addition, two or three bridge piers placed in close proximity have drawn the interest of hydraulic engineers for the safety of the bridge piers. For this concern, some studies were conducted on a group of piers such as [20–26], these studies concluded that if the ratio of pier spacing is 0.25, the resultant scour in SbS arrangement is greater than 50% compared with the single pier. For a ratio of pier spacing less than 0.25, both the piers can be presumed as a single pier. In addition to the above, experimental research on the pier group to examine the spacing impact and countermeasures in scouring depth was conducted by Heidarpour M, Afzalimehr H, Izadinia E, 2010 [27]. Their study concluded that as the distance between the piers

*For correspondence
Published online: 08 June 2022

expands, the region between the piers without protection is washed away, resulting in deeper scour holes at the upstream side of the piers. Behzad and Beheshti [28] investigated the interference between the piers relies on the angle of attack, the geometry of the pier model, and the C2C spacing of piers. The Behzad and Beheshti [28] also investigated the local scour processes in piers with various configurations and distances. Results of work conducted shows that as the C2C spacing between the piers increases, the depth of the scour increases. To explore the flat, protected, and rough bed WU Peng, hirshfield Faye, SUI Jueyi in research work [29] have conducted fifty-four flume tests for evaluating the local scour across the single pier in the open channel. These studies reveal essential information about the behavior of the bridge single and two piers, but they also show that there is not a unified approach for predicting the scour depth for closely placed pier models and the role of pier spacing in the scour depth estimation. Considering these gaps, this research has been scheduled and carried out. The pier spacing (1.5–5 D) was varied with an interval of 0.5 D in order to consider the effect of C2C separation between piers. For assessment of MSD, different equations were used, and results of the equations were validated with the experimental data.

2. Experimental methodology

Testing was carried out in the hydraulic laboratory at Delhi Technological University. The 14 m length and 1.10 m width recirculating flume is fitted with ADV velocimeter and the Venturi meter and has a depth of 0.80 m, represented in figure 1. Venturi meter and ADV, were used to measure the velocity of the flume section. At a distance of 5 m from the inlet tank, a sand recess or working section of 5 m was prepared. The total length of the working section was 5 m which were located at 5 meters from the upstream of the flume. Two cylindrical piers made up of acrylic pipes of diameter D, 5 cm, were used as pier models. These piers were positioned at the center of the working section, which was 7.5 m from the upstream of the flume. The C2C spacing between the piers was 1.5, 2, 2.5, 3, 3.5, 4, 4.5, and 5 times the diameter of the pier. Experimental work was conducted in three sets by increasing the flow rate (0.0295, 0.0428, and 0.0537) m^3/sec under clear water conditions. The working section was prepared with Yamuna sand, with the mean particle size, D_{50}, being 0.60 mm, specific gravity S_g, 2.62, and uniformity coefficient, C_u, is 2, and then curvature coefficient, C_c, is 1. If $C_u < 6$ and $1 < C_c < 3$ for sand, then it will be taken into consideration as uniformly graded [18]. All the flow parameters and experimental conditions are described in table 2. The experimental run time was set to 480 minutes for each experiment, as the scour depth developed after 360 minutes was considered equilibrium scour depth. As per the research work conducted by Setia [30] time needed to achieve an equilibrium scour depth of around 90% was initial 300 minutes, and researchers like [8, 15] have also concluded that maximum scour takes place in the initial 180–240 minutes of the experimental run. Keeping in view the laboratory facilities, the experiment run duration of 480 minutes was fixed for carrying out all the experiments.

Scour depth around the piers was observed every 10 minutes for the initial one hour, and after that, observations were done after every 30 minutes for the next seven hours. The water pump was turned off, and the flume water was drained at the end of each test run. The final bed level measurements were then taken with a vernier point gauge with ± 0.1 mm accuracy. The scour depth was measured on the piers peripheral encircle (upstream, right, left, and

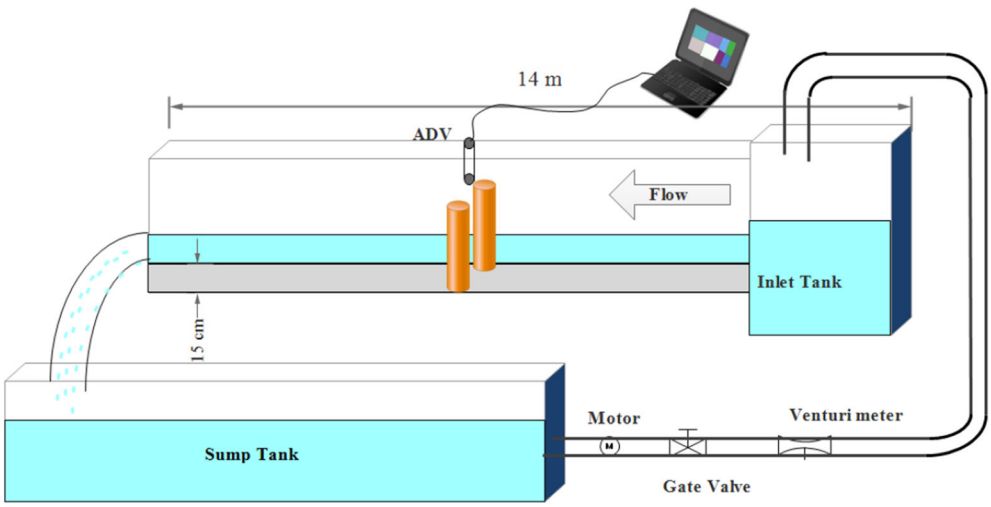

Figure 1. Experimental set up for SbS positioned bridge piers.

downstream). Scour profile was measured at about 20 mm away from the pier along the axis of symmetry as shown in figure 2. It was observed that no significant changes in scouring depth and scouring hole equilibrium depth were found after a lapse of 8 hours. The universal criteria proposed by Melville in his research work [16] need to be satisfied for the experimental conditions such as (a) the ratio of the bed width of the channel, B, to the diameter of a pier, D, should not be less than 6.5 for no channel wall effect or contraction effect, the ratio is equal to 110/5= 22; (b) the ratio of flow depth, H, to the pier diameter, D, should be greater than 3 for independent scour depth, the ratio is equal to 16/5 = 3.2 and (c) the ratio of pier diameter, D, to the mean particle size of sand, D_{50} should be greater than 50 for sediment particle effect, the ratio is equal to 50/0.60 = 83.33 (figure 2).

2.1 *ADV functioning*

The instantaneous 3-D velocity measurement was conducted by utilizing SonTek 16 MHz MicroADV. ADV is a single-point current meter that accurately measures the 3-Dimensional velocity components of water velocity in both high and low flow conditions. The specifications of the ADV are presented in table 1. Velocities are measured in a sampling volume located at a distance away from the probe head. The probe head was made up of a single transmitter located in the center of the probe head. The transmitter generates an acoustic pulse narrow beam that is projected through the water. The reflection of these pulses from the particles or "scatterers" is reflected and received by the ADV receiver. The intersection of the receiver axes designates the location of the sampling volume. There are four types of ADV probes: (i) 3-D down-looking probe, (ii) 3-D up-looking probe, (iii) 3-D side looking probe, and (iv) 2-D side-looking probe. Among these four types of probes, 3-D down-looking probe is employed for this study. In the present study, the x-axis of the down-looking probe indicates the velocity in the direction of flow, downward direction being positive; the y-axis indicates the transverse flow and the z-axis down-flow, downward direction being positive.

SonTek 16 MHz MicroADV with 5 cm distance to Sampling Volume, which had a maximum sampling rate of 50 Hz and volume of 0.09 cc was employed. In our study, the sampling rate for the data collection was selected as 25 Hz. The output data from the ADV were filtered by neglecting the negative values. Depending on the turbulence intensity, the sampling durations were 5 minutes in order to have a statistically time-independent average velocity. The ADV readings were taken at four vertical lines upstream and downstream of the pier and the inlet and outlet at the working section. Each vertical line consists of three horizontal points where ADV reading was recorded at bed level, surface level, and at 0.6 h (average velocity). However, the vertical resolution of the measurements was higher above the scour hole. As a general rule, the velocity range should always be set as small as possible. If, for example, the maximum expected velocity is 8 cm/sec, the velocity range should be set to 10 cm/sec. This is because the noise in the data increases with increasing velocity range and hence loses precision at high sampling rate [31]. In the present study, SonTek's HorizonADV software (v1.20) was utilized for the data collection.

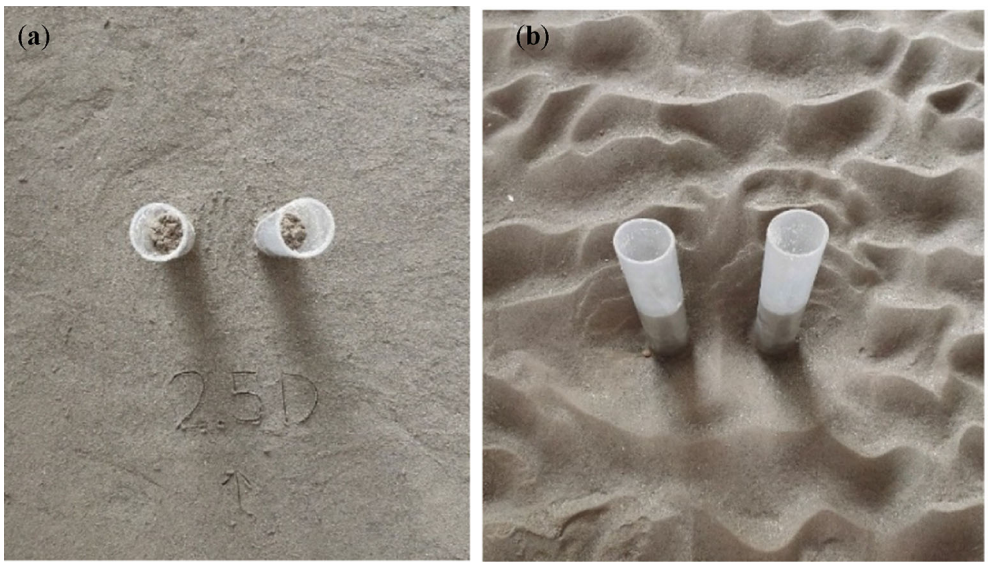

Figure 2. Experimental setup of two piers positioned at 2.5 D spacing in SbS (**a**) before equilibrium scour depth achieved; (**b**) after equilibrium scour depth achieved.

Table 1. ADV specifications.

Sampling Rate	0.1–50 Hz
Sampling Volume	0.09 cc
Distance to Sampling Volume	5 cm
Resolution	0.01 cm/s
Programmed velocity range	3, 10, 30, 100, 250 cm/s
Accuracy	1% of measured velocity, 0.25 cm/s
Maximum Depth	60 m
Temperature Sensor	0.1°C
Compass/Tilt Sensor-Heading, Pitch, Roll Resolution	0.1°
Compass/Tilt sensor-Heading Accuracy	± 2°
Compass/Tilt Sensor-Pitch, Roll Accuracy	± 1°
Pressure Sensor Strain Gauge-Accuracy	0.1%
Resonance Pressure Transducer (RPT)-Accuracy	0.01%
Input Power	12–24 VDC
Typical Power Consumption	2.5–4 W operating

3. Dimensional formulation for the factors affecting MSD around twin piers

For a particular discharge, the scour depth due to the presence of a bridge pier over time reaches a static depth, which is called equilibrium scour depth. The depth of the scour generally associated with the sediment movement with the flow [32]. Overall, the scouring depth across bridge columns depends on different parameters that have been grouped as flow parameters, material bed parameters, and channel geometry parameters. The scour depth can be described by equation (1).

$$\begin{aligned} Y_s = & f_1(\text{Flow parameters}(\rho, \mu, g, V, h, t, t_e)), \\ & f_2(\text{Bed material } (V_c, D, V, d_{50}, \rho_s)), \\ & f_3(\text{Channel geometry } (L, B, H)) \end{aligned} \tag{1}$$

where, variables of function f_1 are, ρ is water density, μ is dynamic viscosity, V is the velocity of flow, h is water depth above the sediment bed, g is the acceleration due to gravity, t is a time of the experimental run, t_e is a time of equilibrium scour depth; variable of function f_2 are, D_{50} is mean particle size, ρ_s density of soil particle, V_c is critical velocity, and variables of function f_3 are, D is the diameter of a pier, L is the length of the channel, B is the width of the channel, H is a depth of the channel (table 2).

From Vaschy Buckingham π theorem, we get:

$$Y_s = f_1\left[\frac{\rho v h}{\mu}, \frac{v^2}{gh}, \frac{t}{t_e}\right], f_2\left[\frac{v_c d_{50}}{v}, \frac{D}{d_{50}}\right], f_3\left[\frac{L}{B}, \frac{H}{B}\right] \tag{2}$$

The term Reynold number ($\frac{\rho V h}{\mu}$) and flow intensity ($\frac{V_c d_{50}}{V}$) are basic parameters considered for bed load. But due to entirely turbulent flow, the effect of the pier Reynolds number and flow intensity on the present study was considered in three sets for varying pier spacing. Thus, for each set of experiments, these two variables are ignored. So, the relative scour depth is a function of the degree of vorticity, $\frac{V^2}{gh}$; relative roughness, $\frac{D}{d_{50}}$; and non-dimensional parameters ($\frac{t}{t_e}$, $\frac{L}{B}$, $\frac{H}{B}$) as given in equation (3).

$$Y_s = f\left[\frac{V^2}{gh}, \frac{t}{t_e}, \frac{D}{d_{50}}, \frac{L}{B}, \frac{H}{B}\right] \tag{3}$$

4. Experimental findings and discussion

4.1 *Effect of the Froude number on the MSD for two piers placed in SbS positioning*

Figure 3 shows the temporal evolution of the scour depth for a single pier as the Froude number increases under the clear-water conditions. These curves shows the dependency of the scour depth on the experimental time, rate of flow and water depth. After the attainment of the dynamic equilibrium scour depth, the scour evolution stopped, but very low transportation of sediment from upstream of the pier to the downstream of the pier still takes place at a very low rate. In the present study, equilibrium state was achieved after 360 minutes. After 360 minutes of experimental run, scour depth approximately becomes constant as presented in figure 3.

Table 2. Flow parameters and experimental conditions.

Set No.	D (mm)	D_{50} (mm)	H (m)	V (m/sec)	Q (m^3/sec)	F_r	R_e	V_c	V/V_c
1	50	0.60	0.120	0.224	0.0295	0.206	30100	0.308	0.72
2	50	0.60	0.149	0.262	0.0428	0.217	43700	0.317	0.83
3	50	0.60	0.163	0.300	0.0537	0.237	54800	0.321	0.93

D = pier diameter; D_{50}= mean particle size; H = flow depth; Q = rate of flow; F_r = Froude number; R_e = Reynolds's number; V_c = Critical Velocity.

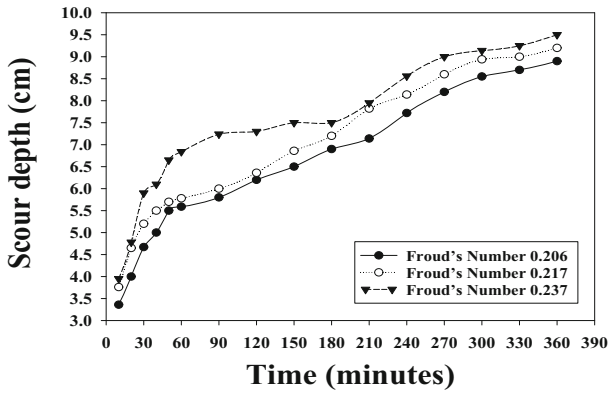

Figure 3. Temporal evolution of MSD across the single pier.

Table 3. Values of Equilibrium time calculated via using equation (3) and equilibrium scour depth extent.

Experimental Set	*h/D*	V/V_c	t_e	Y_t
1	2.4	0.72	2.74	0.9436
2	2.98	0.83	3.33	0.9189
3	3.26	0.93	3.66	0.8975

t_e is the Equilibrium time calculated using equation 3, Y_t is the equilibrium scour depth extent.

An equilibrium time t_e can be provisioned in two ways: firstly, for the last section of the experimental run, at the stage of development and mean scour depth attainment, the equilibrium time was determined. Secondly, equations proposed by Melville and Chiew [12] were opted for forecasting the equilibrium scour depth Y_t. The time factor is defined as the ratio of the scour depth (Y_s) achieved at a time interval t to the equilibrium scour depth upstream of the pier (Y_t) at time t_e. The expression for Y_t is expressed as:

$$\mathrm{Y_t} = \exp\left\{-0.03\left|\frac{\mathrm{V_c}}{\mathrm{V}}\ln\left(\frac{\mathrm{t}}{\mathrm{t_e}}\right)\right|^{1.6}\right\} \tag{4}$$

where $\mathrm{t_e}$ is given as:

$$\mathrm{t_e(days)} = 48.26\frac{\mathrm{D}}{\mathrm{V}}\left(\frac{\mathrm{V}}{\mathrm{V_c}} - 0.4\right) \text{ for } \frac{Y_s}{\mathrm{D}} > 6,\ \frac{\mathrm{V}}{\mathrm{V_c}} > 0.4 \tag{5}$$

$$\mathrm{t_e(days)} = 30.89\frac{\mathrm{D}}{\mathrm{V}}\left(\frac{\mathrm{V}}{\mathrm{V_c}} - 0.4\right)\left(\frac{Y_s}{\mathrm{D}}\right)^{0.25} \text{ for } \frac{Y_s}{\mathrm{D}} < 6, \frac{\mathrm{V}}{\mathrm{V_c}} > 0.4 \tag{6}$$

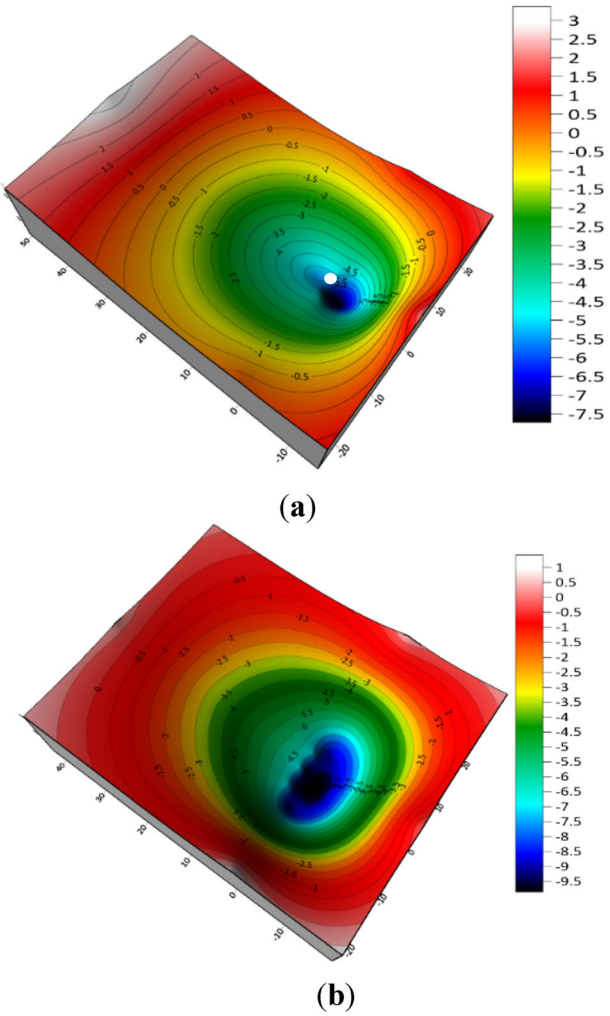

Figure 4. Contours after the equilibrium scour depth (**a**) single pier; (**b**) two piers in SbS positioning.

Here, $y_s/D < 6$, therefore equation (3) opted. For the present study, the values of time factor $\mathrm{Y_t}$ (8 hours) are represented in table 3; the meantime factor was calculated as 92% for the equilibrium scour depth.

The temporal evolution of the MSD for a single pier and twin piers located in SbS positioning with the C2C spacing (1.5D, 2D, 2.5 D, 3D, 3.5D, 4D, 4.5D, and 5D) was tracked. The representation of the temporal evolution of scour depth is shown in figure 3. Figure 3 shows that the scour depths $\mathrm{Y_t}$ were established speedily during the initial 480 minutes period and about 92 percent of overall scour depth was attained.

The higher the Froude number more significant will be the corresponding MSD. The dimensionless shear pressure increases with the Froude number [33]. Therefore, the finer the sediment of the river bed, lower will be the dimensional shear stress resulting in sediment movement. Due to this

reason scouring depths will be greater for increasing Froude numbers.

4.2 *Effect of sediment deposition patterns on MSD for two piers*

The amount of the sediment transported from the upstream of the piers gets deposited on downstream of the pier in the form of a deposition mound. The depth of the scour hole upstream, and the interaction of horseshoe and wake vortices influence the deposition of silt on the mound of bridge piers. Results showed that the greater the mound height downstream of the pier, the rate of flow between two piers would also be more pronounced. Owing to the existence of a scour hole and the reverse vector magnitudes, the relationship between the shear layers weakens in the wake of the pier. For each pier on the downstream side, wake vortices does not overlap with each other. For validation of this flow, visualization experiments [25] were conducted for instantaneous and average velocity, vorticity, and Reynold stress contour and streamline topology using PIV technologies. The experimental results show that the behavior of the cylinders is asymmetrical at a slight gap ratio due to the jet-like circulation between the cylinders in this side-by-side arrangement. The free surface and scour depth inside the scour hole for each pier also show independence of wake vortices [21]. As the initial surface level is lowered from its original bed level, this increases the flow space of water. The existence of a scour hole starts speeding up the flow into the scouring hole by reducing the frictional effect. This affects the movement of the sediments between the two piers. The findings demonstrate that the maximum scour depths have been found on the upstream side of the bridge piers. The upstream downflow of the pier is similar to a vertical jet that erodes an area facing the pier [34].

The wake vortex works like a vacuum cleaner, which collects sediment materials from the horseshoe vortex and deposits the sediment downstream the pier. Sediment is deposited on the bridge piers in the shape of a mound of deposit. The scour hole depth is visible in the contour plot as shown in figure 4 on the front of the bridge piers. At the stage of equilibrium scour, most of the flow passes through

Table 4. Experimental results on the upstream side of the pier for the side-by-side arrangement.

Run No.	Q	(C_s)	(Y_{su})	(Y_{sul})	(Y_{sur})	(Y_{sul}/Y_{su})	(Y_{sur}/Y_{su})
1	0.0295	0	89				
2	0.0428	0	92				
3	0.0537	0	95				
4	0.0295	1.5 D		81	80.8	0.91	0.91
5	0.0295	2 D		80	79	0.90	0.89
6	0.0295	2.5 D		81	80	0.91	0.90
7	0.0295	3 D		78	77.8	0.88	0.87
8	0.0295	3.5 D		72	72.5	0.81	0.81
9	0.0295	4 D		70.4	71.2	0.79	0.80
10	0.0295	4.5 D		69	70.5	0.78	0.79
11	0.0295	5 D		68.4	69	0.77	0.78
12	0.0428	1.5 D		83.5	83.6	0.91	0.91
13	0.0428	2 D		82	81.6	0.89	0.89
14	0.0428	2.5 D		83	83	0.90	0.90
15	0.0428	3 D		80	80.2	0.87	0.87
16	0.0428	3.5 D		74.7	74.2	0.81	0.81
17	0.0428	4 D		72.3	72.25	0.79	0.79
18	0.0428	4.5 D		70	70.4	0.76	0.77
19	0.0428	5 D		67.4	67.3	0.73	0.73
20	0.0537	1.5 D		85.6	85.5	0.90	0.90
21	0.0537	2 D		82	83	0.86	0.87
22	0.0537	2.5 D		85.4	85.2	0.90	0.90
23	0.0537	3 D		84	84.2	0.88	0.89
24	0.0537	3.5 D		80.7	80.4	0.85	0.85
25	0.0537	4 D		74	73.2	0.78	0.77
26	0.0537	4.5 D		71	70.8	0.75	0.75
27	0.0537	5 D		70	69.6	0.74	0.73

C_s is the clear space between the piers in mm, Y_{su} is the Scour depth upstream for the single pier in mm, Y_{sul} is the Scour depth on the upstream of the left pier in mm, Y_{sur} is the Scour depth on the upstream of the right pier in mm.

Table 5. Experimental results on the downstream side of the pier for the side-by-side arrangement.

Run NO.	Q	(C_s)	(Y_{sd})	(Y_{sdl})	(Y_{sdr})	(Y_{sdl}/Y_{sd})	(Y_{sdr}/Y_{sd})
1	0.0295	0	68				
2	0.0428	0	73				
3	0.0537	0	76				
4	0.0295	1.5 D		46	45.2	0.68	0.66
5	0.0295	2 D		48	49	0.71	0.72
6	0.0295	2.5 D		42.4	42	0.62	0.62
7	0.0295	3 D		40.3	40.2	0.59	0.59
8	0.0295	3.5 D		36	35.2	0.53	0.52
9	0.0295	4 D		34.1	33.8	0.50	0.50
10	0.0295	4.5 D		32.4	32.8	0.48	0.48
11	0.0295	5 D		30.8	30.1	0.45	0.44
12	0.0428	1.5 D		54.5	54.5	0.75	0.75
13	0.0428	2 D		62	62	0.85	0.85
14	0.0428	2.5 D		53.7	54.5	0.74	0.75
15	0.0428	3 D		51.7	50	0.71	0.68
16	0.0428	3.5 D		50.3	50.1	0.69	0.69
17	0.0428	4 D		48.7	49	0.67	0.67
18	0.0428	4.5 D		47	47	0.64	0.64
19	0.0428	5 D		45	45	0.62	0.62
20	0.0537	1.5 D		67	67.4	0.88	0.89
21	0.0537	2 D		68.5	68.3	0.90	0.90
22	0.0537	2.5 D		62.4	62.3	0.82	0.82
23	0.0537	3 D		60.4	60.2	0.79	0.79
24	0.0537	3.5 D		54	52.1	0.71	0.69
25	0.0537	4 D		53	53.2	0.70	0.70
26	0.0537	4.5 D		52	51.4	0.68	0.68
27	0.0537	5 D		50	50.2	0.66	0.66

C_s is the Clear Space between the piers in mm, Y_{sd} is the Scour depth downstream for the single pier in mm, Y_{sdl} is the Scour depth downstream of the left pier in mm, Y_{sdr} is the Scour depth on downstream of the right pier in mm

the piers near the actual bed, and the deflection of flow outside the piers was reduced. During the initial experimentation stage, the water flow between the piers acts as a water jet. These jet stars erode the sediment from the pier spacing region and deposit this on the downstream side. After the evolution of the equilibrium scour hole, this rate of erosion and transportation in the pier spacing region gets reduced. The resultant equilibrium scour hole for MSD has been presented in figure 4. The existence of jet flow between the two piers partially reduces when the equilibrium scour depth achieved. The flow divergence around the piers on the outer region of scour hole becomes negligible at equilibrium state, and that is represented in figure 4(a) and (b).

In both cases, the maximum negative z value (intensive downflow) was located upstream of the pier, but the maximum scour depth was achieved for the twin pier placed at 1.5 D, as shown in figure 4(b). These values are higher upstream and are linked to the influence of the inside scour hole. Upward flow is noticed at the wake of the pier, and the flow is then directed to the bed on the sides of the pier and the wake region for continuity of the flow. There was a heavier drop in the scour between the two piers than on the outside of the piers [21].

4.3 *Effect of spacing between the piers on the scour pattern around the two piers*

The experimental results of SbS positioned for MSD are tabulated below. Table 4 represents the MSD outcomes on the upstream side, and table 5 illustrates the MSD on the downstream side of the pier. Tables 4 and 5 also illustrate the non-dimensional scour depth findings for the upstream and downstream of the pier, respectively.

The evolution of the scour hole near the pier results from the sediment transportation phenomenon and 3-D characteristic flow. Firstly, due to the water flow around the piers undergoing 3-D separation. After that, individual shear layers start revolving around the pier and initiate the vortex formation upstream of the pier. This vortex formation is known as horseshoe vortex as it appears like a horseshoe from the top view. Due to the forming of horseshoe vortex and down flow near the pier, sediment transportation rate and shear stress increases. This led to the evolution of scour holes around the pier, and consequently, variation in flow pattern was observed, resulting in a decrease of shear stress and sediment transportation [35]. The MSD depends on the strength of the horseshoe vortex; the strength of the horseshoe vortex is dependent on flow turbulence so, flow

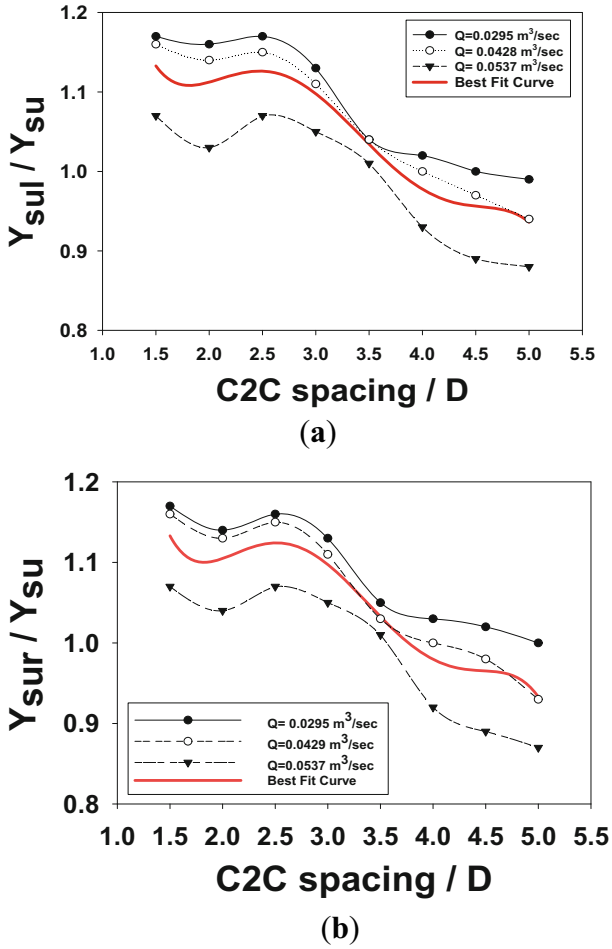

Figure 5. Normalized scour depth on the upstream of piers versus normalized C2C spacing between piers (**a**) left pier and (**b**) Right pier.

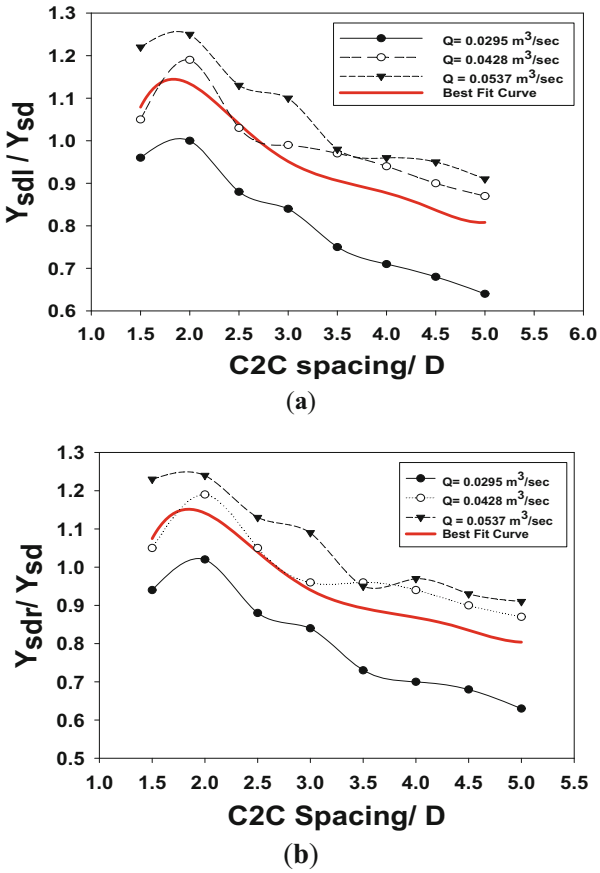

Figure 6. Normalized scour depth on the downstream of piers versus normalized C2C spacing between piers (**a**) left pier and (**b**) Right pier.

turbulence is directly dependent on the Reynolds number (R_e). Hence as a result of this correlation, the intensity of the horseshoe vortex is directly proportional to the Reynolds number of the pier (R_e). The resulting MSD decreases with an increase in the C2C pier spacing, and the intensity of horseshoe vortexes decreases. Thus, greater the pier spacing C2C spacing lower will be turbulence and enormous will be the horseshoe vortices, resulting into the growth of scour hole.

The pattern of the MSD on the upstream side of both the left and right piers is pretty similar, and evidence is represented in figure 5. Figure 5(a) and (b) represent normalized scour depth against the normalized C2C spacing between the left and right pier, respectively. The trend of both the curves is similar, and it shows that as we increase the C2C spacing, the mutual interdependence of the piers is reduced. Similarly, with the increase in the flow discharge, the depth of scouring is increased. This trend is projected as a rational 2nd-degree quadratic equation in equation (7) for the best fit curve with global goodness of fit R^2 for the left pier curve is 0.994. Similarly, equation (8) represents the best fit curve with global goodness of fit R^2 for the right pier curve is 0.9877.

$$Y_{sul} = \frac{a_1 + b_1 x + c_1 x^2}{1 + d_1 x + e_1 x^2} \tag{7}$$

where values of constants in equation (7) are such as: a_1 =1.0781, b_1= −0.5481, c_1= 0.0793, d_1= −0.5225, e_1 = 0.0780

$$Y_{sur} = \frac{a_2 + b_2 x + c_2 x^2}{1 + d_2 x + e_2 x^2} \tag{8}$$

where values of constants in equation (8) are such as: a_2 = 1.0693, b_2 = −0.5590, c_2 = 0.0828, d_2 = −0.5370, e_2 = 0.0819

The trend for the upstream side of piers is similar for both the piers, similar trend was perceived on the downstream of both the piers represented in figure 6. Figure 6(a) and (b) represent normalized scour depth against the normalized C2C spacing between the left and right pier, respectively. Both the piers behaved identically for three sets of experimental runs and curves plotted for the

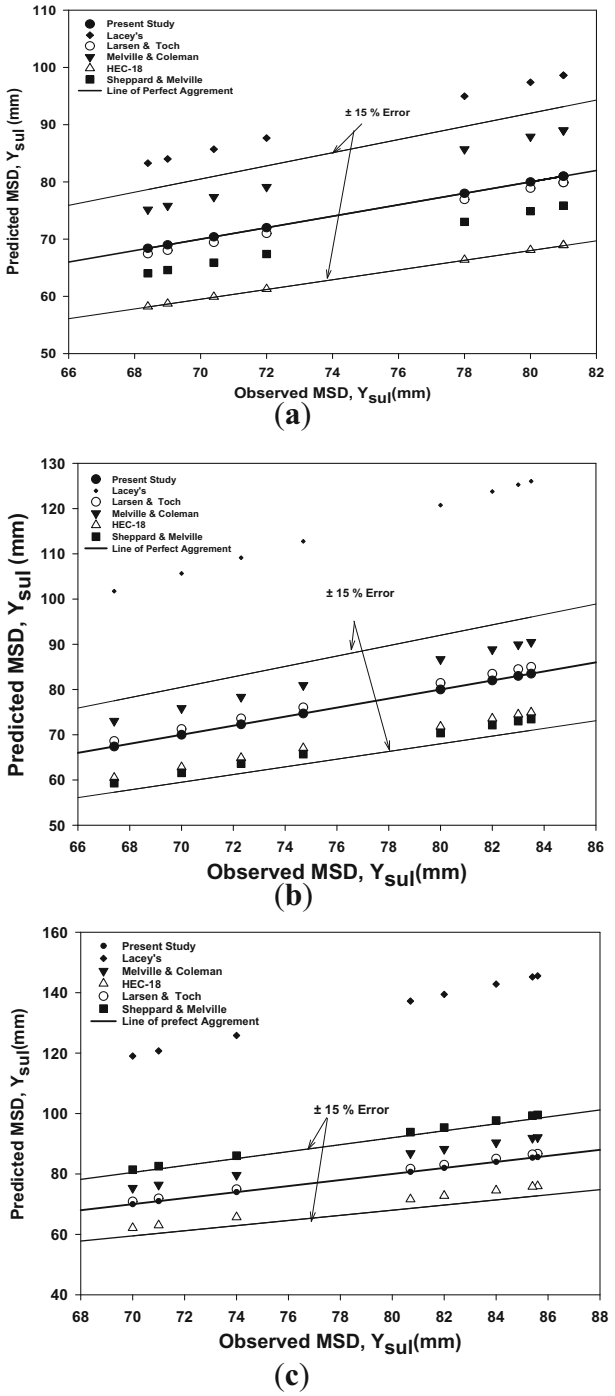

Figure 7. Observed versus predicted MSD on upstream of the left pier for Froude number (**a**) 0.206, (**b**) 0.217 and (**c**) 0.237.

normalized scour depth against the normalized C2C spacing between the piers and best-fitted curves represented. This trend is projected similarly as opted for upstream side, and concerned equations are represented. Equation (9) represents the best-fit curve for the left pier on the downstream side with global goodness of fit R^2 = 0.9605. Similarly, equation (10) represents the best fit curve with global goodness of fit R^2 for the right pier curve is 0.9475.

$$Y_{sdl} = \frac{a_3 + b_3 x + c_3 x^2}{1 + d_3 x + e_3 x^2} \tag{9}$$

where values of constants in equation (9) are such as: a_3 =1.4423, b_3 = −0.6195, c_3= 0.0035, d_3 = −0.2713, e_3 = −0.0647

$$Y_{sdr} = \frac{a_4 + b_4 x + c_4 x^2}{1 + d_4 x + e_4 x^2} \tag{10}$$

where values constants in equation are such as: a_4 =1.5107, b_4 = −0.5773, c_4 = −0.0100, d_4 = −0.1851, e_4 = −0.0852.

The curves presented in figure 6 shows a gradual decline in the scour depth with the increase in clear spacing between the piers and scour depth increases with the increases in the rate of flow. The two piers behave identically when they are placed side-by-side with each other and, when placed in very close proximity,they behave like one pier of larger diameter size, and as a result, the scour depth for the close spacing was higher than the single pier. C2C was more significant when the spacing was three times the diameter of the pier. At C2C, spacing equal to 3D piers started behaving individually, and scour depth decreased. Minimum scour depth was attained at the maximum C2C spacing that is 5D.

4.4 *Evaluation of MSD using semi-empirical equations*

For predicting the MSD across the bridge pier, the observed scour depth was multiplied by the spacing factor. The experimental scour depth across the piers was not the same as predicted values, which undoubtedly increases the difficulty of scour prediction. Therefore, a factor of pier spacing is defined as (P_s). P_{sul} and P_{sur} are the pier spacing factors for the left and right pier, respectively, for an upstream side of piers.

$$Y_{sul} = P_{sul} Y_s \tag{11}$$

$$Y_{sur} = P_{sur} Y_s \tag{12}$$

The observed experimental results of equilibrium scour depth at the upstream and downstream for all the pier arrangements were compared with the predicted results from semi-empirical equations.

Scour depth at the upstream of both the piers was calculated using the above expressions of the results of the traditional equations. Figure 7(a), (b), and (c) represent the MSD for the experimental results versus the predicted results of five well-known equations for the left pier. These plots concluded that the prediction ability of the IRC equation was almost double than the observed MSD as the factor of safety is very high. It can be used for structures where a higher factor of safety is needed. For accurately predicting the scour depth, these equations are lined as the

Table 6. List of semi-empirical equations used in the present study.

	Expression
Melville and Coleman	$Y_s = K_{yb}K_1K_dK_sK_\theta K_gK_t$ where, Y_s = Local scour depth below the bed level (m), K_{yb} = Factor of pier size for flow depth, K_1 = Factor of flow Intensity, K_d = Factor of sediment size, K_s = Factor of foundation shape, K_θ = Factor of foundation alignment, K_g = Factor of approach channel geometry, K_t = Factor of time.
HEC-18 Federal Highway Administration (FHwA)	$\frac{Y_s}{h_u} = 2.0k_1k_2k_3k_w\left(\frac{D}{h_u}\right)^{0.65} F^{0.43}$ where: Y_s = Scour depth (m), h_u = Head of flow on upstream of the pier (m), D = Diameter of pier (m), K_1, K_2, K_3 and K_w = Factors of correction, F = Froude number, g = Acceleration due to gravity, V = Mean velocity of flow (m/s).
IRC (1998 &2000):	$Y_s = 0.473\left(Q/f\right)^{1/3}, \quad when \frac{L}{B} \geq 1$ $Y_s = 1.34\left(\frac{q^2}{f}\right)^{1/3}, \quad when \frac{L}{B} \leq 1$ where; Q = Design discharge (m^3/sec), Y_s = Scour depth (m), q = Intensity of discharge (m^3/s/m), Q/L & f = Silt factor given by Lacey's equation, L = Clear waterway (m), and B = Mean width of channel (regime width) (m).
S/M Equation or Sheppard and Melville equation	$\frac{y_s}{D} = 2.5f_1f_2f_3 \quad for\ 0.4 \leq \frac{V}{V_c} \leq 1.0$ $\frac{y_s}{D} = f_1\left[2.2\left(\frac{\frac{v}{v_c}-1}{\frac{v_{lp}}{v_c}-1}\right) + 2.5f_3\left(\frac{\frac{v_{lp}}{v_c}-\frac{v}{v_c}}{\frac{v_{lp}}{v_c}-1}\right)\right] \quad for\ 1 \leq \frac{V}{V_c} \leq \frac{V_{lp}}{V_c}$ $\frac{Y_s}{D} = 2.2f_1 \quad for\ \frac{V}{V_c} > \frac{V_{lp}}{V_c}$ where, Y_s = Scour depth below the bed level (m), D = Diameter of pier (m), f_1, f_2, f_3 = S/M's coefficients, V = Mean velocity of flow (m/s), V_c = Critical Velocity of flow (m/s), V_{IP} = Live bed peak velocity of flow (m/s).
Larsen and Toch	$Y_s = 1.35\ D^{0.7}\ h^{0.3}$ where Y_s = Scour depth below the bed level (m), D = Diameter of the pier (m), and h = Head of flow (m)

S/M equation, Larsen and Toch equation, Melville and Coleman, HEC-18, and IRC (Lacey's equation). The MSD prediction trend for the left and right pier for the side-by-side arrangement was observed similar to each other. Out of five semi-empirical equations Larsen and Toch and S/M equation were observed as the best suitable equation for the present study (table 6).

Figures 8(a), (b), and (c) represent the MSD for the observed experimental results versus predicted results by using the five well-known equations for the right pier. The trends of MSD around the right pier were similar to the left pier, and the prediction ability of equations was also similar. The best suitable equation for the present experimental data was Larsen and Toch and S/M equation. Maximum predicted scour depth was calculated using equations (11) and (12), and the results were compared with the experimental scour depth in order to find out the statistical errors. All the equations, with the exception of the Lacey equation, agreed with the experimental findings within the ± 15% Normalized Root Mean Square Error (NRMSE) range presented in table 7.

4.5 *Error statistics*

In addition to the experimental data, statistical parameters such as Normalized Root Mean Square Error (NRMSE), Mean Absolute Percentage Error (MAE), and R square Correlation for all the equations are presented in table 7. The method/equation with the least total error and under-prediction is the best performer. A mathematical study of the observed and predicted data was performed to determine the best equation. According to statistical analysis, the Larsen and Toch Equation is the best performing equation that provides the most precise local scour depth. Except for the IRC (Lacey's) equation, the rest of the four equations are lying under ± 15 % error bars, which is an acceptable range as proposed by the author in [36], so these equations can be considered for predicting the MSD around the twin piers placed in the transverse direction of flow. Use of Larsen and Toch, HEC-18, and Melville and Coleman Equations are highly recommended based on error statistics for the precise prediction of the MSD around the two piers placed in the transverse direction of flow despite varying spacing between the piers.

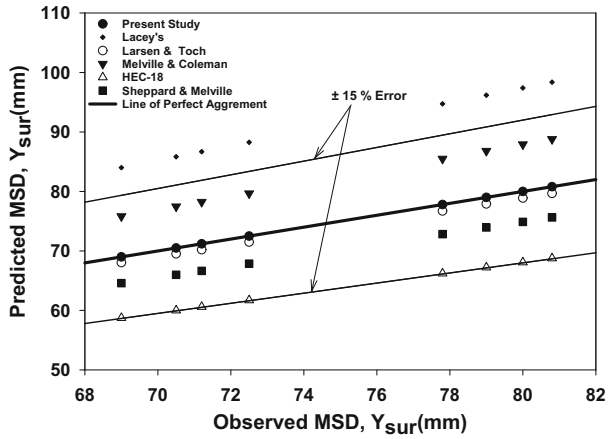

(**a**)

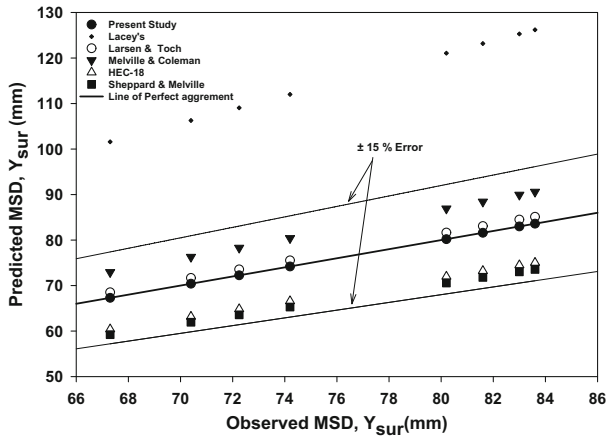

(**b**)

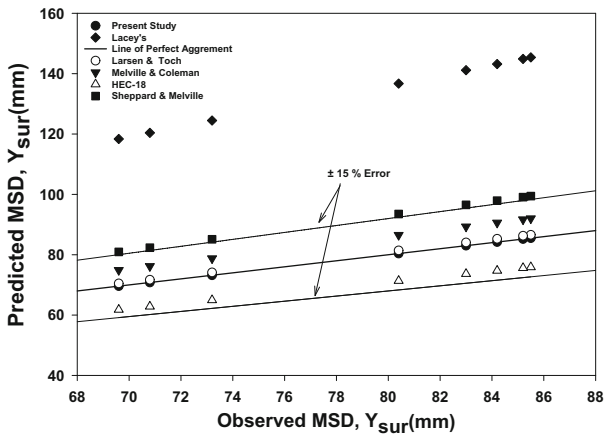

(**c**)

Figure 8. Observed versus predicted MSD on upstream of the right pier for Froude number (**a**) 0.206, (**b**) 0.217 and (**c**) 0.237.

4.6 *Discussion*

In this analysis, the effects of a flow pattern of the piers in the SbS positioning are comparable to the behavior of the twin pier, which changes with the C2C between the piers. We may conclude from the results of this study that the mutual interference among the pier has a direct relationship with the Froude Number and Reynolds number. The horseshoe vortex is extended deeper by the two piers on the upstream side. The flow intensity between the two piers is always higher, and the scouring hole developed is more extensive, so longitudinal and circumferential movement between the piers is impacted. The scour pattern, including the contracted flow and interference between horseshoe vortices, played an essential part in producing and forming a higher scouring depth between the two piers. The existence of the two piers directly impacts the behavior of vortices. The findings are graphically represented, and few mathematical equations have been chosen to validate the experimental results. Experimental results and Larsen and Toch's predicted results are ideally suited for the present study. The experimental results of this study can validate any numerical modeling and computational modeling methods. These experimental results can be in the future for validating any CFD tools.

Table 7. Statistical errors for the side-by-side arrangement.

Arrangement	Analysis results	NRMSE	MAPE	R^2
U/s scour for left pier	IRC	0.525	47.6	0.446
	Melville and Coleman	0.087	8.6	0.988
	HEC-18	0.123	12.1	0.933
	Larsen and Toch	0.015	1.5	0.973
	S/M equation	0.125	11.6	0.437
U/s scour for right pier	IRC	0.525	47.6	0.434
	Melville and Coleman	0.087	8.6	0.987
	HEC-18	0.123	12.1	0.93
	Larsen and Toch	0.015	1.5	0.972
	S/M equation	0.125	11.6	0.431

5. Conclusion

A series of experiments evaluated the effect of mutual interference between the two piers situated in the transverse direction of the flow. This study presents the principal conclusions and are given as follows.

- The extent of scouring at the upstream and downstream sides of the left and right piers was approximately similar. In the case of a SbS arrangement, both the piers behaved were identical. By increasing the spacing between the piers strength of the horseshoe vortices decreases, hence mutual interference will be reduced; this reduction concludes that for larger spacing between the piers, small will be the scour depth and vice versa. The smaller the spacing between the piers, the more enormous will be the interference and scour depth between the piers.

- Piers behaved as a single pier when they were placed in close proximity to each other for spacing less than 2.5D. Scouring at the upstream side increased due to these pier interactions. For the left and right pier, the maximum upstream scour was observed for the C_s = 2.5–3 times D. The minimum scour depth was evaluated for the C_s = 4.5 times D. Scour depth on the downstream side of the pier for both left, and a right pier was maximum for C_s = 1.5 times D and minimum for the C_s = 4.5 times D.
- There is a larger, substantial upflow in the separation between the two piers (especially in the downstream portion of the gap), but a smaller transverse-deflection is formed in contrast to the zone behind the single pier. The flow rate reaching the downstream pier near the bed reduces to 0.2–0.3 V. In the scouring hole at the base of the piers, the highest downflow was observed. The downflow intensity, vertical turbulence, shear stress, and kinetic energy between piers are greater than across the piers.F
- To assess variables impacting MSD, dimensional analysis using the theorem Buckingham π was conducted. So, the parameters that play a vital role in the MSD assessment are: degree of vortices, relative roughness, equilibrium scour depth time, and flow section.
- Five traditional equations were used for predicting the scour depth accurately. Comparison with observed experimental results was made with the ultimate asymptotic scour depth forecast by the suggested equations. Among the five equations used, Larsen and Toch and Sheppard and Melville, HEC-18 and Melville equations predict the scour depth for the mean absolute error percentage of less than 15%. IRC recommended equation overestimated MSD. This equation may be considered for the design in case of a high degree of freedom.

List of symbols

B	Width of the channel
C_c	Curvature coefficient
C_s	Clear space between the piers
C_u	Uniformity coefficient
D	Pier diameter
d_{50}	Mean particle size
F_r	Froude number
g	Acceleration due to gravity
H	Head of water flows over the sand bed
L	Length of the channel
P_{suL}	Pier spacing factors for the left
P_{suR}	Pier spacing factors for the right pier
Q	Rate of flow
R_e	Reynolds number
S_g	Specific gravity
t	Time of the experimental run
t_e	Time at which equilibrium scour depth attained
V	Velocity of flow
V_c	Critical velocity
Y_s	Scour depth
Y_{sd}	Scour depth downstream for the single pier
Y_{sdl}	Scour depth downstream of the left pier
Y_{sdr}	Scour depth on downstream of the right pier
Y_{su}	Scour depth upstream for the single pier
Y_{sul}	Scour depth on the upstream of the left pier
Y_{sur}	Scour depth on the upstream of the right pier
Y_t	Equilibrium scour depth
μ	Dynamic viscosity
ρ	Water density
ρ_s	Density of soil particle

Acknowledgements

This research was funded by the Delhi Technological University, New Delhi, India. Data availabilityThe data used in this research article is experimental data conducted in the Hydraulics Laboratory of the Civil Engineering Department, Delhi Technological University New Delhi, India.

References

[1] Tang H-W, Ding B, Chiew Y-M and Fang S-L 2009 Protection of bridge piers against scouring with tetrahedral frames. *Int. J. Sedim. Res.* 24: 385–399

[2] Pu J H, Wallwork J T, Khan M, Pandey M, Pourshahbaz H, Satyanaga A, Hanmaiahgari P R and Gough T 2021 Flood suspended sediment transport: Combined modelling from dilute to hyper-concentrated flow. *Water (Switzerland)* 13: 1–24

[3] Pandey M, Jamei M, Karbasi M, Ahmadianfar I and Chu X 2021 Prediction of maximum scour depth near spur dikes in uniform bed sediment using stacked generalization ensemble Tree-based frameworks. *J. Irrig. Drain. Eng.* 147: 04021050

[4] Pandey M, Valyrakis M and Qi M *et al.* 2021 Experimental assessment and prediction of temporal scour depth around a spur dike. *Int. J. Sedim. Res.* 36: 17–28

[5] Reza Namaee M and Sui J 2019 Local scour around two side-by-side cylindrical bridge piers under ice-covered conditions. *Int. J. Sedim. Res.* 34: 355–367

[6] Laursen E M and Arthur T 1956 Scour around bridge piers and abutments. Iowa Highway Research Board, Ames

[7] Breusers H N C, Nicollet G and Shen H W 1977 Local scour around cylindrical piers. *J. Hydraul. Res.* 15: 211–252

[8] Yanmaz A M and Altinbilek H D 1991 Study of time-dependent local scour around bridge piers. *J. Hydraul. Eng.* 117: 1247–1268

[9] Kothyari U C and Kumar A 2010 Temporal variation of scour around circular bridge piers. *ISH J. Hydraul. Eng.* 16: 35–48

[10] Melville B W 1997 Pier and abutment scour: Integrated approach. *J. Hydraul. Eng. ASCE* 123(2): 125–136
[11] Martfn-Vide J P, Hidalgo C and Bateman A 1998 Local scour at piled bridge foundations. *J. Hydraul. Eng.* 124: 439–444
[12] Melville B W and Chiew Y 1999 Time scale for local scour at bridge piers. *J. Hydraul. Eng.* 125(1): 59–65
[13] Richardson E V and Davis S R 2001 *Evaluating scour at bridges*
[14] Oliveto G and Hager W H 2002 Temporal evolution of clear-water pier and abutment scour. *J. Hydraul. Eng.* 128(9): 811–820
[15] Mia M F and Nago H 2003 Design method of time-dependent local scour at circular bridge pier. *J. Hydraul. Eng.* 129: 420–427
[16] Chang W, Lai J, Yen C and Asce F 2004 Evolution of scour depth at circular bridge piers. *J. Hydraul. Eng.* 130(9): 905–914
[17] Melville B W 2007 Local scour at bridge abutments. *J. Hydraul. Eng.* 118: 615–631
[18] Arneson L A, Zevenbergen L W, Lagasse P F and Clopper P E 2012 *Evaluating scour at bridges*
[19] Jain R, Lodhi A S, Oliveto G and Pandey M 2021 Influence of cohesion on scour at piers founded in clay–sand–gravel mixtures. *J. Irrig. Drain. Eng.* 147: 04021046
[20] Coleman S E 2005 Clearwater local scour at complex piers. *J. Hydraul. Eng.* 131(4): 330–334
[21] Ataie-Ashtiani B and Aslani-Kordkandi A 2012 Flow field around side-by-side piers with and without a scour hole. *Eur. J. Mech. B/Fluids* 36: 152–166
[22] Amini D, Ataie-ashtiani B and Beheshti A 2018 Prediction of current-induced local scour around complex piers: Review, revisit, and integration. *Coast. Eng.* 133: 43–58
[23] Muzzammil M and Gangadhariah T 2010 The mean characteristics of horseshoe vortex at a cylindrical pier. *J. Hydraul. Res.* 41: 285–297
[24] Muzzammil M, Alama J and Danish M 2015 Scour prediction at bridge piers in cohesive bed using Gene Expression Programming. In: *International conference on water resources, coastal and ocean engineering: Aquatic Procedia*. Elsevier B.V., pp 789–796
[25] Akilli H, Akar A and Karakus C 2004 Flow characteristics of circular cylinders arranged side-by-side in shallow water. *Flow Meas. Instrum.* 15: 187–197
[26] Sumner D, Wong S S T, Price S J and Païdoussis M P 1999 Fluid behaviour of side-by-side circular cylinders in steady cross-flow. *J. Fluids Struct.* 13: 309–338
[27] Heidarpour M, Afzalimehr H and Izadinia E 2010 Reduction of local scour around bridge pier groups using collars. *Int. J. Sedim. Res.* 25: 411–422
[28] Behzad A-A and Beheshti A A 2006 Experimental investigation of clear-water local scour at pile groups. *J. Hydraul. Eng.* 132(10): 1100–1104
[29] Peng W U, Faye H and Jueyi S U I *et al*. 2014 Impacts of ice cover on local scour around semi-circular bridge abutment. *J. Hydrodyn.* 26: 10–18
[30] Setia B 2008 Equilibrium scour depth time. In: *3rd IASME / WSEAS Int. Conf. on Water Resources, Hydraulics & Hydrology (WHH '08),* University of Cambridge, UK,. pp 114–117
[31] Sarker A 1998 Flow measurement around scoured bridge piers using Acoustic-Doppler Velocimeter (ADV). *Flow Meas. Instrum.* 9: 217–227
[32] Coleman B S E and Melville B W 2001 Case study: New Zealand bridge scour experiences. *J. Hydraul. Eng.* 127: 535–546
[33] Wu P, Hirshfield F and Sui J 2015 Armour layer analysis of local scour around bridge abutments under ice cover. *River Res. Appl.* 31: 736–746
[34] Hafez Y I 2016 Mathematical modeling of local scour at slender and wide bridge piers. *J. Fluids* 2016: 1–19
[35] Pandey M, Zakwan M, Khan M A and Bhave S 2020 Development of scour around a circular pier and its modelling using genetic algorithm. *Water Sci. Technol. Water Supply* 20: 3358–3367
[36] Qi M, Li J and Chen Q 2018 Applicability analysis of pier-scour equations in the field: Error analysis by rationalizing measurement data. *J. Hydraul. Eng.* 144: 04018050